Biochemical and Biophysical Research Communications 437 (2013) 12–17

Contents lists available at SciVerse ScienceDirect

Biochemical and Biophysical Research Communications

journal homepage: www.elsevier.com/locate/ybbrc

Structure of the second RRM domain of Nrd1, a fission yeast MAPK target RNA binding protein, and implication for its RNA recognition and regulation

Ayaho Kobayashi [a], Teppei Kanaba [a], Ryosuke Satoh [b], Toshinobu Fujiwara [b,c], Yutaka Ito [a], Reiko Sugiura [d], Masaki Mishima [a,*]

[a] Graduate School of Science and Engineering, Tokyo Metropolitan University, Minamiosawa 1-1, Hachioji 192-0397, Japan
[b] Institute of Microbial Chemistry, 3-14-23 Kamiosaki, Shinagawa-ku 141-0021, Tokyo, Japan
[c] Graduate School of Pharmaceutical Sciences, Nagoya City University, 3-1 Tanabe-dori, Mizuho-ku,Nagoya 467-8603, Japan
[d] Laboratory of Molecular Pharmacogenomics, School of Pharmaceutical Sciences, Kinki University, 3-4-1 Kowakae, Higashi-Osaka 577-8502, Japan

ARTICLE INFO

Article history:
Received 26 May 2013
Available online 12 June 2013

Keywords:
Nrd1
MAPK
RRM
Phosphorylation

ABSTRACT

Negative regulator of differentiation 1 (Nrd1) is known as a negative regulator of sexual differentiation in fission yeast. Recently, it has been revealed that Nrd1 also regulates cytokinesis, in which physical separation of the cell is achieved by a contractile ring comprising many proteins including actin and myosin. Cdc4, a myosin II light chain, is known to be required for cytokinesis. Nrd1 binds and stabilizes Cdc4 mRNA, and thereby suppressing the cytokinesis defects of the *cdc4* mutants. Interestingly, Pmk1 MAPK phosphorylates Nrd1, resulting in markedly reduced RNA binding activity. Furthermore, Nrd1 localizes to stress granules in response to various stresses, and Pmk1 phosphorylation enhances the localization. Nrd1 consists of four RRM domains, although the mechanism by which Pmk1 regulates the RNA binding activity of Nrd1 is unknown. In an effort to delineate the relationship between Nrd1 structure and function, we prepared each RNA binding domain of Nrd1 and examined RNA binding to chemically synthesized oligo RNA using NMR. The structure of the second RRM domain of Nrd1 was determined and the RNA binding site on the second RRM domain was mapped by NMR. A plausible mechanism pertaining to the regulation of RNA binding activity by phosphorylation is also discussed.

1. Introduction

Negative regulator of differentiation 1 (Nrd1), also known as multicopy suppressor of sporulation abnormal mutant 2 (Msa2), is a negative regulator of sexual differentiation in fission yeast [1–3]. Nrd1 blocks the onset of sexual differentiation by repressing a series of Ste11-regulated genes essential for conjugation and meiosis. Sequence analysis suggested that Nrd1 consists of four RRM domains, and biochemical analysis showed that Nrd1 preferentially binds poly(U) sequences, although the cellular target mRNA is unknown [1]. One mammalian functional counterpart identified is regulator of differentiation 1 (ROD1), which suppresses lethality of the temperature-sensitive Pat1 (a protein kinase inhibits sexual differentiation by phosphorylating the meiotic inducer Mei2 and the transcription factor Ste11) mutant (*pat1-114ts*) [4]. ROD1 is a protein with four RRM domains with its ability to repress Ste11-regulated genes and to inhibit conjugation upon overexpression [4].

Recently, it has been revealed that Nrd1 is a regulator of cytokinesis. Physical separation of the cell is achieved by a contractile ring comprising many proteins including actin and myosin. Among these, Cdc4 is known as an essential myosin II light chain in fission yeast and is required for cytokinesis [5–7]. Nrd1 has been identified as a multicopy suppressor of the temperature-sensitive *cdc4* mutant [8]. Nrd1 regulates cytokinesis by enhancing myosin mRNA stability through direct binding and stabilization of Cdc4 mRNA [8]. Importantly, Pmk1, a MAPK in fission yeast [9], phosphorylates Nrd1. Thr40 in the N-terminal region and Thr126 in the first RRM domain of Nrd1 are known to be phosphorylated by Pmk1, and these Pmk1-dependent phosphorylations significantly reduce its RNA binding activity [8]. Pmk1 MAPK signaling thus regulates cytokinesis by posttranscriptional level regulation of *cdc4* [8]. The UCUU motif in the Cdc4-coding region of the

Abbreviations: RRM, RNA recognition motif; IPTG, isopropyl β-D-1-thiogalactopyranoside; GST, glutathione S-transferase; TCEP, tris(2-carboxyethyl)phosphine; NOE, nuclear Overhauser effect; NOESY, NOE spectroscopy; TOCSY, total correlation spectroscopy; HSQC, heteronuclear single quantum correlation spectroscopy.

* Corresponding author. Fax: +81 42 677 2525.
E-mail address: mishima-masaki@tmu.ac.jp (M. Mishima).

0006-291X/$ - see front matter © 2013 Elsevier Inc. All rights reserved.
http://dx.doi.org/10.1016/j.bbrc.2013.06.008

mRNA is a candidate for the Nrd1 target RNA binding sequence, the mutation of which resulted in a significant reduction in Nrd1 binding affinity [8]. Furthermore, Nrd1 forms RNA granules in response to various stresses, and is a key component of stress granules (SGs) which coordinate stress responses and SG formation. Nrd1 binds Cpc2, a RACK homologue in fission yeast, in a phosphorylation-dependent manner, and its localization to stress granules is modulated by MAPK phosphorylation [10]. Nrd1 also shares significant sequence similarity and a common preferred RNA-binding sequence (UCUU) with mammalian proteins T-cell-restricted intracellular antigen-1 (TIA-1) and TIA-1-related protein (TIAR), which play a key role in SG assembly in response to adverse environmental stimuli [11,12].

In an effort to reveal the relationship between structure and function of Nrd1, we prepared samples of each RRM domain and qualitatively examined RNA binding activity using NMR. As a contribution towards the structural analysis of full-length Nrd1, we initially determined the structure of the second RRM domain of Nrd1. Here, we report on the solution structure of the second RRM domain of Nrd1 and its RNA binding site revealed by NMR. We also discuss a plausible mechanism relating to the regulation of Nrd1 by phosphorylation.

2. Materials and methods

2.1. Sample preparation

RRM1, RRM2, RRM3 and RRM4, comprising Nrd1 residues 108–191, 188–284, 309–412 and 397–501, respectively, were each cloned into the plasmid pET49b(+) (Novagen) and expressed in *Escherichia coli* cells as fusion proteins containing GST and HRV3C cleavage sites at the N-terminus. Uniform labeling of these proteins with ^{15}N or ^{15}N and ^{13}C was achieved using M9 minimal medium containing $^{15}NH_4Cl$ and [$^{13}C_6$]-glucose as the sole source of nitrogen and carbon, respectively. Each protein was expressed and purified as follows. Cells were grown at 37 °C and protein expression was induced by the addition of IPTG when the absorbance at 660 nm was 0.5. Cells were then cultured at 20 °C for 16 h prior to harvesting. Harvested wet cells were resuspended in 50 mM Tris–HCl (pH 8.0) buffer containing 400 mM KCl, 0.1 mM EDTA and 1 mM DTT. The cell suspension was lysed by sonication, ultra-centrifuged, and the supernatant loaded onto a Glutathione Sepharose Fast Flow (GE Healthcare) affinity column. The N-terminal GST was then removed by treatment with HRV3C proteinase. The protein was further purified by passage through a Superdex 75 gel-filtration column (GE Healthcare). Sample homogeneity was checked by SDS–PAGE.

2.2. NMR spectroscopy and structure calculation

The RRM2 samples employed for structural determination by NMR were dissolved in 50 mM K-phosphate (pH 6.0) buffer containing 100 mM KCl, 0.1 mM EDTA and 1 mM TCEP in either 93% H_2O/7% ^2H_2O or 99.8% ^2H_2O. The final protein concentrations were 0.35–0.9 mM. NMR spectra were acquired at 30 °C on a Bruker AVANCE III 600 NMR spectrometer equipped with a TCI cryogenic probe. Data were processed using NMRPipe [13], and NMR spectra were analyzed using Sparky [14]. The ^1H, ^{13}C and ^{15}N assignments were mainly obtained from standard multidimensional NMR methods, HNCACB, CBCA(CO)NH, HN(CA)CO and HNCO for main-chain assignments, and C(CO)NH, H(CCO)NH, HCCH-TOCSY and 4D HC(CO)NH for side-chain assignments [15,16]. Aromatic ^1H and ^{13}C assignments were obtained from 3D ^{13}C edited NOESY-HSQC. Methyl groups of Leu and Val residues of RRM2 were assigned in a stereospecific manner using a ^1H–^{13}C constant-time HSQC spectrum of a 10% ^{13}C randomly enriched protein sample [17]. Stereospecific assignment of β-methylene and $\chi1$ rotamer were determined from HNHB and HACAHB [18,19]. Inter-proton distances were derived from 3D ^{15}N edited NOESY-HSQC, and 3D ^{13}C edited NOESY-HSQC. Backbone dihedral ϕ and ψ angles were derived from TALOS+ [20].

The program CYANA using the CANDID protocol was used for structural restraint collection [21]. An ensemble of 100 RRM2 structures were calculated using the program CNS version 1.2 by a standard simulated annealing protocol [22]. Finally, structures were refined using a water refinement protocol [23]. The final 20 ensemble structures with the lowest energy were checked by PROCHECK-NMR [24] and MolProbity [25]. Molecular graphics were generated using PyMOL [26]. The lowest energy structure among the ensemble was used as representative in order to compare structures and generate a ribbon model. The atomic coordinates have been deposited in the PDB with the accession code 2RT3.

2.3. RNA binding analysis

Chemical shift perturbations of ^1H and ^{15}N amide resonances of ^{15}N uniformly labeled RRM1, RRM2 and RRM4 were monitored upon addition of an excess amount of RNA. The NMR sample contained 0.1 mM of each protein in K-phosphate (pH 6.0) buffer containing 100 mM KCl, 1 mM TCEP, 0.1 mM EDTA and 7% ^2H_2O. The ^1H–^{15}N HSQC experiments were performed at 30 °C. For each cross-peak, the weighted average shift difference δ_{ave} was calculated. The weighted average shift difference δ_{ave} was calculated as $\{[(\delta_{1H})^2 + (\delta_{15N})^2/25]\}^{1/2}$, where δ_{1H} and δ_{15N} represent the difference in ppm between the free and perturbed chemical shifts. Chemical shift changes were analyzed using Sparky [14].

3. Results and discussion

3.1. Preparation and characterization of each RRM domain

We constructed *E. coli* expression systems for RRM1 (108–191), RRM2 (188–284), RRM3 (309–412) and RRM4 (397–501), and purified the proteins. We measured ^1H–^{15}N HSQC spectra for the RRM1–RRM4 proteins, and RRM1, RRM2 and RRM4 provided well dispersed signals. NMR signals of RRM3 were difficult to detect possibly due to heavy broadening, and purification of the RRM3 protein was problematic. The RRM3 protein eluted in the void volume during gel-filtration, indicating the presence of protein aggregates (data not shown). We next examined the RNA binding character and RNA binding site of RRM1, RRM2 and RRM4 using NMR. To this end, chemical shift perturbation (CSP) experiments were performed. Since the interactions were weak, an excess amount of chemically synthesized non-labeled RNA (5-mer; UUCUU) was added to the ^{15}N-labeled proteins (the molar ratio of the each protein to RNA was 1:4) in the CSP experiments. As a result, changes in the chemical shift of a number of peaks of RRM2 were observed, while signals of RRM1 and RRM4 were not significantly perturbed (Fig. 1A and B). This suggests that RRM2 may play an important role in the interaction between Nrd1 and target mRNA, although the possibility that RRM3 possesses RNA binding activity cannot yet be excluded. The RRM2 domain was then subjected to structural analysis and mapping of the RNA binding site.

3.2. Structure determination of RRM2

Purified RRM2 domain provided well dispersed signals with relatively narrow line shape in the ^1H–^{15}N HSQC spectrum as shown (Fig. 1B), and the elution volume in the gel-filtration corresponded to a molecular weight of the monomer (data not shown).

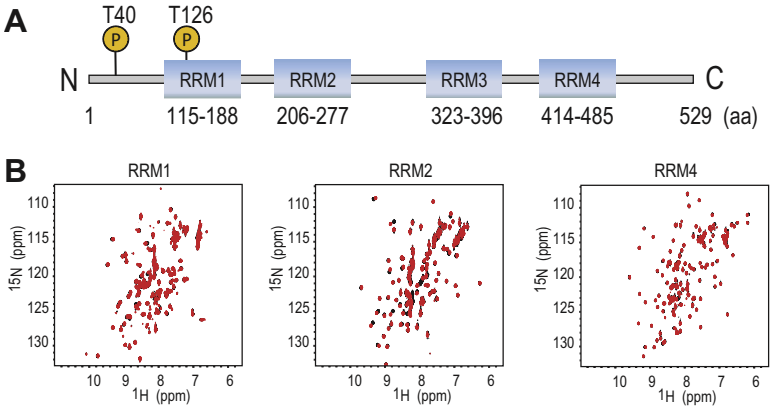

Fig. 1. Domain organization of Nrd1 and binding to UUCUU monitored by NMR. (A) Four RRMs (RNA recognition motifs) and Thr residues (Thr40 and Thr126) phosphorylated by Pmk1 are indicated in the schematic cartoon of Nrd1. The domain boundaries are determined according as EXPASY (http://www.expasy.org). (B) ^{1}H–^{15}N HSQC spectra of the ^{15}N-labeled RRM1, RRM2 and RRM4 domains shown on the left, middle and right, respectively. The spectra of RNA-free and 4-fold excess non-labeled UUCUU are shown in black and red, respectively, and superimposed.

These results indicated that RRM2 exists as a monomer in solution. Almost all ^{1}H, ^{13}C, and ^{15}N NMR signals were assigned using standard multi-dimensional NMR techniques.

The number of distance restraints derived from NOE was sufficient (more than two thousand), and the ensemble of 20 structures were in excellent agreement with a large body of experimental data (Fig. 2A) (Table S1). The r.m.s. deviations of the backbone and all heavy atoms of RRM2 are 0.18 and 0.53 Å, respectively, excluding disordered regions. In particular, the conformation of the N-terminal (residues 188–203) and C-terminal (275–284) regions of RRM2 are not converged (Fig. 2A).

RRM2 comprises an anti-parallel β-sheet and four α-helices. The β-sheet is composed of four β-strands, β1 (residues 207–211), β2 (233–238), β3 (242–248) and β4 (272–274). The short α-helix, α1 (196–200), is located distal to the core region of the protein while the other three α-helices, α2 (219–229), α3 (251–263) and α4 (266–269), pack against the β-sheet (Fig. 2A and B). Although the first short helix α1 is shown close to the core region of the RRM2 domain in the ribbon model (Fig. 2B), this part is not converged in the ensemble and is highly mobile in the solution state as indicated by the ^{1}H–^{15}N heteronuclear NOE experiment (Fig. 2A and C).

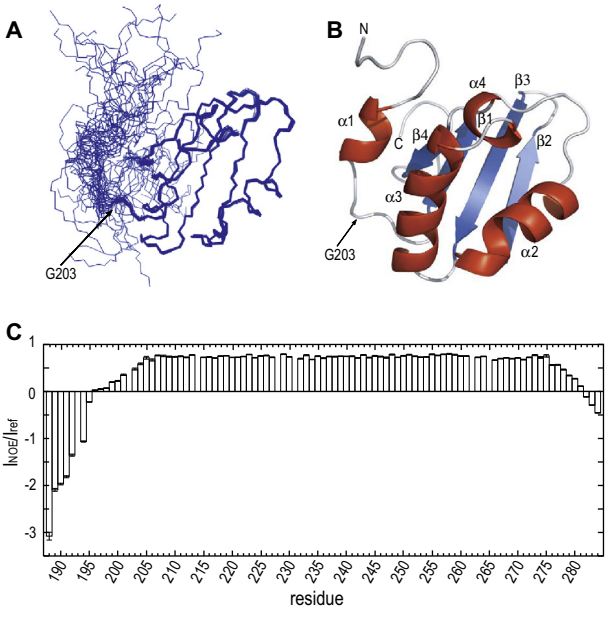

Fig. 2. Solution structure of the RRM2 domain. (A) Backbone superposition of the final 20 simulated annealing structures of RRM2. (B) Ribbon drawing of a representative structure of the RRM2 domain. The molecular orientation is the same as in (A) with the four-stranded β-sheet and four α-helices depicted in blue and red, respectively. α-helices and β-strands are labeled. The position of Gly203 is indicated with an arrow (A and B). (C) {^{1}H}–^{15}N NOE versus amino acid residue for RRM2. The data are represented by the intensity ratio I_{NOE}/I_{ref}, where I_{ref} and I_{NOE} were measured in the absence or presence of ^{1}H saturation, respectively. The error bars were calculated based on the signal-to-noise ratios.

3.3. Structure comparison

The overall structure adopts a fold typically observed in canonical RRMs. A DALI database search, which quantitatively evaluates tertiary structure similarities, showed that the structure of the RRM2 domain resembles that of hnRNP (PDB code: 3R27), Nab3 (PDB code: 2XNR), Pre-mRNA-splicing factor RBM22 (PDB code: 2YTC), U1 small nuclear ribonucleoprotein A (PDB code: 1OIA), Tra2-β (PDB code: 2RRB) and Raver1 (PDB code: 3H2V), with highest *Z*-scores of 10.4, 9.8, 9.7, 9.7, 9.7 and 9.6, respectively.

Among the proteins showing high similarity to RRM2, a structure comparison between RRM2 and Nab3 is of critical importance since Nab3 shares the same RNA binding sequence preference (UCUU) as RRM2. Notably, the RRM2 domain of Nrd1 is well fitted to the RRM domain of Nab3 in complex with UCUU (PDB code: 2XNR), and displaying a low r.m.s. deviation (1.4 Å for backbone coordinates by DALI). In the Nab3–UCUU complex, the side-chains of Phe333 and Ser400 are stacked against the cytosine base, and Phe366 and Phe368 contact the ribose of the cytosine. The hydroxyl group of Ser399 hydrogen bonds to the cytosine base, and backbone amide of Ser400 and backbone carbonyl of Val398 also recognize the cytosine base [27]. Additionally, Glu397 and Asn361 form hydrogen bonds to the first and third uridine bases, respectively (Fig. 3) [27]. In comparison, Phe209, Ile243 and Phe245 are present within the β-sheet of RRM2, which correspond to Phe333, Phe366 and Phe368 of Nab3, respectively (Fig. 3). In the last (fourth) β-strand and C-terminal region of RRM2, Tyr273, Tyr274, Gly275 and Arg276 are present which correspond to Glu397, Val398, Ser399 and Ser400 of Nab3, respectively (Fig. 3).

Taken together, it could be concluded that the key residues for RNA binding are mostly conserved in RRM2, although the Asn361, Glu397 and Ser399 in Nab3 are substituted to Lys236, Tyr273 and Gly275 in RRM2, respectively. This may result in loss of hydrogen bonds with the bases observed in the Nab3–RNA complex in part, and may account at least in part for the observed weak binding of RRM2 to RNA.

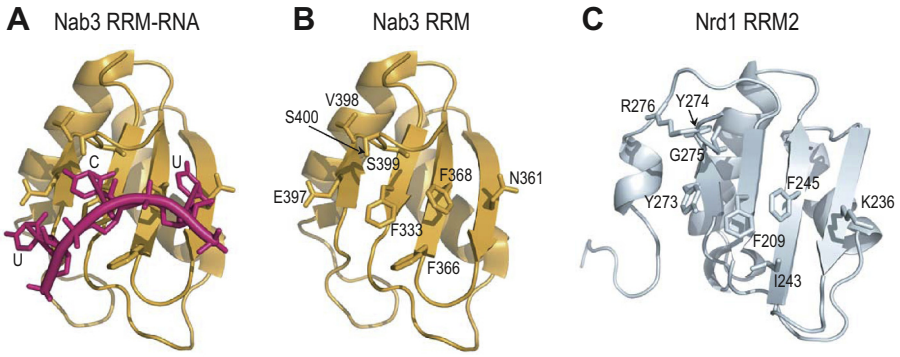

Fig. 3. Structure comparison of the Nrd1 RRM2 domain with the Nab3 RRM domain. (A) Crystal structure of the Nab3 RRM domain/RNA (UCUU) complex (PDB code: 2XNR). The Nab3 RRM domain and RNA are colored yellow and magenta, respectively. (B) Nab3 RRM domain residues important for the recognition of RNA are shown in stick representation and labeled. (C) Solution structure of the Nrd1 RRM2 domain colored in cyan. The molecular orientation is the same as for Nab3. Corresponding residues to the Nab3 residues important for the recognition of RNA are shown in stick representation and labeled. C-terminal 7 residues are omitted for clarity.

The RRM1 domain of Raver1, which also shows high structural similarity to RRM2, plays a role in protein–protein interactions with the tail of the cytoskeletal protein Vinculin. Lee et al. reported the structure of the RRM1 domain of Raver1 in complex with Vinculin [28]. However, it seems that the Vinculin-like local protein–protein interaction interface is absent in the RRM2 domain of Nrd1, although there is remarkable similarity in the overall structure as indicated by DALI (Fig. S1).

3.4. Mapping of RNA interaction site of RRM2

The RNA binding site of the RRM2 domain was estimated by mapping the significant chemical shift changes of the amide signals of the HSQC spectra of RRM2. Upon addition of RNA, some signals of RRM2 were significantly perturbed in a fast-exchange manner, resulting in changes in chemical shift (Fig. 4A). We mapped the distribution of significantly perturbed residues on the molecular surface of RRM2 and found that these residues were confined to the β-sheet, suggesting that the β-sheet represents the RNA binding site (Fig. 4B and C). The location of this RNA binding site is consistent with other RRM domains such as that of Nab3 (Fig. 3). As revealed by structure comparison with the Nab3–UCUU complex, most of the key residues required for RNA recognition are conserved in RRM2, and some these key residues, including Ile243 and Phe245, are actually perturbed upon RNA binding (Fig. 4B and C). The other conserved residue, Phe209, was not significantly perturbed, although flanking residue 210 is significantly perturbed upon RNA binding. Since the backbone amide NMR signal is the probe for this experiment, the change in chemical shift of residue 210 may reflect perturbation of the closely located side-chain of Phe209 upon RNA binding. In the fourth β-strand and C-terminal region, residues Tyr273, Arg276 and Asp277 are significantly perturbed upon RNA binding (Fig. 4B and C).

3.5. Functional implications

Overall, the RRM2 domain structure seems to reflect a typical RRM domain. In this study, only RRM2 showed marked changes in chemical shift upon RNA binding in a fast-exchange manner, which is typically observed in cases of weak binding. Structure determination and DALI searches revealed that RRM2 and Nab3 are very similar. With the structure comparison of the RNA binding site between RRM2 and Nab3, we presumed that RRM2 employs a similar RNA recognizing mechanism to Nab3. In fact, chemical shift perturbation upon RNA binding was observed for the conserved residues and their neighbors.

It is puzzling that the reported phosphorylation of Nrd1 residues by Pmk1, which inhibits RNA binding, occurs at residue positions not located within RRM2, but within the N-terminal region (Thr40) and RRM1 domain (Thr126) (Fig. 1A). Thus, the mechanism by which phosphorylation inhibits RNA binding cannot be explained by a simple mechanism such as steric hindrance of the RNA molecule resulting from the presence of a phosphate moiety on the RRM2 domain. Rather, it is plausible that Nrd1 adopts an autoinhibited structure by a rearrangement of domain orientation.

Our NMR structural study revealed that the N-terminal region (188–203) of RRM2 behaves independently relative to the core region of RRM2. It probably acts as a hinge around Gly203 (Fig. 2A and C). Therefore, the relative orientation between RRM1 and RRM2 is probably mobile given this hinge. One possible mechanism of regulation of Nrd1 by Pmk1 involves phosphorylation-induced rearrangement of domain orientation around the hinge and subsequent adoption of an auto-inhibitory form. RRM1 or some other region of Nrd1 may mask the RNA binding site of Nrd1 by inter-domain interactions induced by phosphorylation. Notably, inter-RRM domain interactions have been reported for U2AF65 [29], although there is no significant homology with the RRM2 domain of Nrd1. Prediction of disordered regions using the program PrDos suggested that Nrd1 possesses some flexible regions in addition to the N- and C-terminal regions (Fig. S2). In particular, flexible region 1 (residues 190–199 located between RRM1 and RRM2), which almost corresponds to the experimentally identified hinge region, flexible region 2 (residues 288–311 located between RRM2 and RRM3), and flexible region 3 (residues 404–410 located between RRM3 and RRM4) showed high scores (Fig. S2). Interestingly, RRM1, RRM2 and RRM4 showed low scores, consistent with the fact that the NMR spectra of RRM1, RRM2 and RRM4 comprised well dispersed signals, indicating the presence of folded structures. Together with information concerning the experimentally identified domains and hinge region, and the prediction of disordered regions, we presume that Nrd1 adopts a beads-on-a-string structure, whereby each RRM domain is linked by flexible hinges (linkers) comprising flexible regions 1–3. These domains may undergo phosphorylation-induced changes in orientation by utilizing these flexible hinges.

Future studies will need to be directed towards the structural analysis of phosphorylated and non-phosphorylated full-length Nrd1. For analysis of phosphorylation-induced domain rearrangement of the full-length protein, NMR and small angle X-ray scattering (SAXS) are powerful tools that can be utilized in addition to X-ray crystal structure analysis [30]. Rigorous quantitative RNA binding studies involving each RRM domain and full-length protein

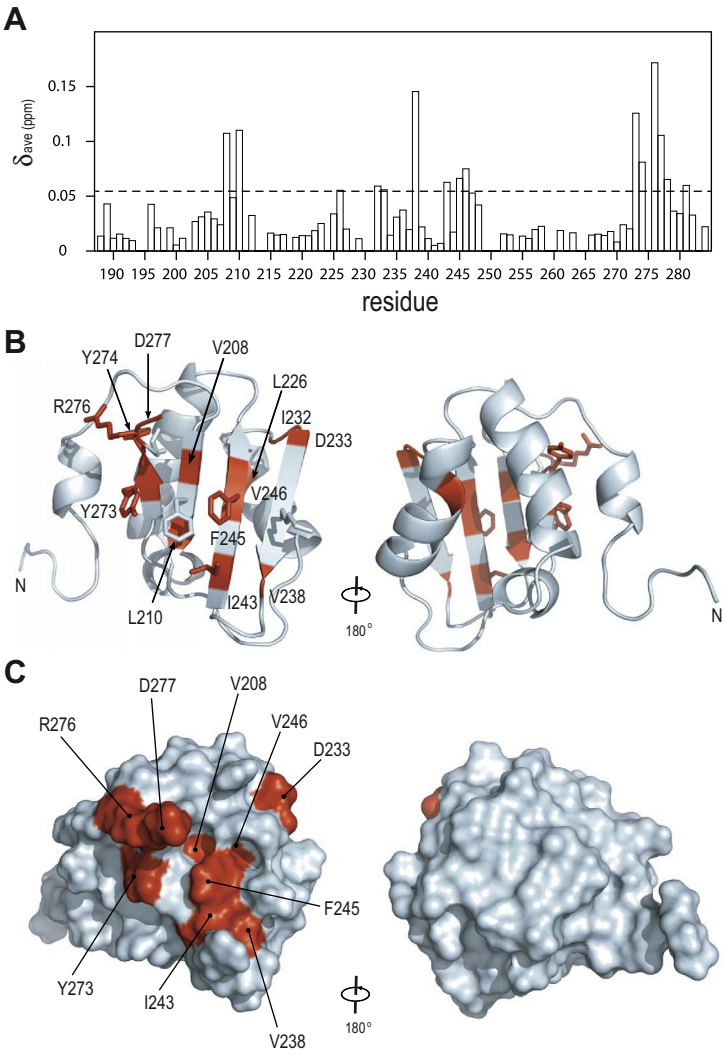

Fig. 4. RNA binding site of the RRM2 domain. (A) Weighted average of ^{1}H and ^{15}N chemical shift perturbations of residues in RRM2 induced by Cdc4 mRNA (UUCUU) binding. The dashed line indicates the threshold for mapping. (B, C) Significantly perturbed residues are mapped on the ribbon drawing (B) and on the molecular surface model (C) of the RRM2 structure. Residues significantly perturbed are highlighted in red and labeled. C-terminal 7 residues are omitted for clarity.

may also be useful in delineating the mechanism involved in the regulation of Nrd1 activity.

Acknowledgments

This work was supported by a Grant-in-Aid for Scientific Research on Innovative Areas, Protein Modifications in Pathogenic Dysregulation of Signaling, Structural Cell Biology and Transient Macromolecular Complex KAKENHI GRANT numbers 25117723, 22121001, 22121002, 22121516 and 24121722 from MEXT (to M.M.).

Appendix A. Supplementary data

Supplementary data associated with this article can be found, in the online version, at http://dx.doi.org/10.1016/j.bbrc.2013.06.008.

References

[1] K. Tsukahara, H. Yamamoto, H. Okayama, An RNA binding protein negatively controlling differentiation in fission yeast, Mol. Cell. Biol. 18 (1998) 4488–4498.

[2] H.T. Jeong, F. Ozoe, K. Tanaka, T. Nakagawa, H. Matsuda, M. Kawamukai, A novel gene, msa1, inhibits sexual differentiation in *Schizosaccharomyces pombe*, Genetics 167 (2004) 77–91.

[3] H.T. Jeong, Y. Oowatari, M. Abe, K. Tanaka, H. Matsuda, M. Kawamukai, Interaction between a negative regulator (Msa2/Nrd1) and a positive regulator (Cpc2) of sexual differentiation in *Schizosaccharomyces pombe*, Biosci. Biotechnol. Biochem. 68 (2004) 1621–1626.

[4] H. Yamamoto, K. Tsukahara, Y. Kanaoka, S. Jinno, H. Okayama, Isolation of a mammalian homologue of a fission yeast differentiation regulator, Mol. Cell. Biol. 19 (1999) 3829–3841.

[5] D.A. Guertin, S. Trautmann, D. McCollum, Cytokinesis in eukaryotes, Microbiol. Mol. Biol. Rev. 66 (2002) 155–178.

[6] M.C. Hou, D. McCollum, Cytokinesis: myosin spots the ring, Curr. Biol. 12 (2002) R334–336.

[7] D. McCollum, M.K. Balasubramanian, L.E. Pelcher, S.M. Hemmingsen, K.L. Gould, *Schizosaccharomyces pombe* cdc4+ gene encodes a novel EF-hand protein essential for cytokinesis, J. Cell Biol. 130 (1995) 651–660.

[8] R. Satoh, T. Morita, H. Takada, A. Kita, S. Ishiwata, A. Doi, K. Hagihara, A. Taga, Y. Matsumura, H. Tohda, R. Sugiura, Role of the RNA-binding protein Nrd1 and Pmk1 mitogen-activated protein kinase in the regulation of myosin mRNA stability in fission yeast, Mol. Biol. Cell 20 (2009) 2473–2485.

[9] T. Toda, S. Dhut, G. Superti-Furga, Y. Gotoh, E. Nishida, R. Sugiura, T. Kuno, The fission yeast pmk1+ gene encodes a novel mitogen-activated protein kinase homolog which regulates cell integrity and functions coordinately with the protein kinase C pathway, Mol. Cell. Biol. 16 (1996) 6752–6764.

[10] R. Satoh, A. Tanaka, A. Kita, T. Morita, Y. Matsumura, N. Umeda, M. Takada, S. Hayashi, T. Tani, K. Shinmyozu, R. Sugiura, Role of the RNA-binding protein Nrd1 in stress granule formation and its implication in the stress response in fission yeast, PLoS ONE 7 (2012) e29683.

[11] N.L. Kedersha, M. Gupta, W. Li, I. Miller, P. Anderson, RNA-binding proteins TIA-1 and TIAR link the phosphorylation of eIF-2 alpha to the assembly of mammalian stress granules, J. Cell Biol. 147 (1999) 1431–1442.
[12] L.M. Dember, N.D. Kim, K.Q. Liu, P. Anderson, Individual RNA recognition motifs of TIA-1 and TIAR have different RNA binding specificities, J. Biol. Chem. 271 (1996) 2783–2788.
[13] F. Delaglio, S. Grzesiek, G.W. Vuister, G. Zhu, J. Pfeifer, A. Bax, NMRPipe: a multidimensional spectral processing system based on UNIX pipes, J. Biomol. NMR 6 (1995) 277–293.
[14] T.D. Goddard, D.G. Kneller, SPARKY3, University of California, San Francisco, 1999.
[15] M. Sattler, J. Schleucher, C. Griesinger, Heteronuclear multidimensional NMR experiments for the structure determination of proteins in solution employing pulsed field gradients, Prog. Nucl. Magn. Reson. Spectrosc. 34 (1999) 93–158.
[16] R.T. Clowes, W. Boucher, C.H. Hardman, P.J. Domaille, E.D. Laue, A 4D HCC(CO)NNH experiment for the correlation of aliphatic side-chain and backbone resonances in 13C/15N-labelled proteins, J. Biomol. NMR 3 (1993) 349–354.
[17] D. Neri, T. Szyperski, G. Otting, H. Senn, K. Wuthrich, Stereospecific nuclear magnetic resonance assignments of the methyl groups of valine and leucine in the DNA-binding domain of the 434 repressor by biosynthetically directed fractional 13C labeling, Biochemistry 28 (1989) 7510–7516.
[18] S.J. Archer, M. Ikura, D.A. Torchia, A. Bax, An alternative 3D NMR technique for correlating backbone 15N with side-chain Hb resonances in larger proteins, J. Magn. Reson. 95 (1991) 636–641.
[19] S. Grzesiek, H. Kuboniwa, A.P. Hinck, A. Bax, Multiple-quantum line narrowing for measurement of H-alpha-H-beta J-couplings in isotopically enriched proteins, J. Am. Chem. Soc. 117 (1995) 5312–5315.
[20] Y. Shen, F. Delaglio, G. Cornilescu, A. Bax, TALOS+: a hybrid method for predicting protein backbone torsion angles from NMR chemical shifts, J. Biomol. NMR 44 (2009) 213–223.
[21] T. Herrmann, P. Guntert, K. Wuthrich, Protein NMR structure determination with automated NOE assignment using the new software CANDID and the torsion angle dynamics algorithm DYANA, J. Mol. Biol. 319 (2002) 209–227.
[22] A.T. Brunger, P.D. Adams, G.M. Clore, W.L. DeLano, P. Gros, R.W. Grosse-Kunstleve, J.S. Jiang, J. Kuszewski, M. Nilges, N.S. Pannu, R.J. Read, L.M. Rice, T. Simonson, G.L. Warren, Crystallography & NMR system: a new software suite for macromolecular structure determination, Acta Crystallogr. D 54 (1998) 905–921.
[23] J.P. Linge, M.A. Williams, C.A. Spronk, A.M. Bonvin, M. Nilges, Refinement of protein structures in explicit solvent, Proteins 50 (2003) 496–506.
[24] R.A. Laskowski, J.A. Rullmannn, M.W. MacArthur, R. Kaptein, J.M. Thornton, AQUA and PROCHECK-NMR: programs for checking the quality of protein structures solved by NMR, J. Biomol. NMR 8 (1996) 477–486.
[25] V.B. Chen, W.B. Arendall III, J.J. Headd, D.A. Keedy, R.M. Immormino, G.J. Kapral, L.W. Murray, J.S. Richardson, D.C. Richardson, MolProbity: all-atom structure validation for macromolecular crystallography, Acta Crystallogr. D: Biol. Crystallogr. 66 (2010) 12–21.
[26] W.L. DeLano, The PyMOL Molecular Graphics System, 2002.
[27] B.M. Lunde, M. Horner, A. Meinhart, Structural insights into cis element recognition of non-polyadenylated RNAs by the Nab3-RRM, Nucleic Acids Res. 39 (2011) 337–346.
[28] J.H. Lee, E.S. Rangarajan, S.D. Yogesha, T. Izard, Raver1 interactions with vinculin and RNA suggest a feed-forward pathway in directing mRNA to focal adhesions, Structure 17 (2009) 833–842.
[29] C.D. Mackereth, T. Madl, S. Bonnal, B. Simon, K. Zanier, A. Gasch, V. Rybin, J. Valcarcel, M. Sattler, Multi-domain conformational selection underlies pre-mRNA splicing regulation by U2AF, Nature 475 (2011) 408–411.
[30] J. Hennig, I. Wang, M. Sonntag, F. Gabel, M. Sattler, Combining NMR and small angle X-ray and neutron scattering in the structural analysis of a ternary protein-RNA complex, J. Biomol. NMR (2013).